Available online at www.sciencedirect.com
ScienceDirect
Journal of Catalysis 246 (2007) 177–192
JOURNAL OF CATALYSIS
www.elsevier.com/locate/jcat

Steam reforming of methanol over copper-containing catalysts: Influence of support material on microkinetics

B. Frank [a], F.C. Jentoft [b], H. Soerijanto [a,b], J. Kröhnert [b], R. Schlögl [b], R. Schomäcker [a,*]

[a] *Institute of Chemistry, TU Berlin, Secr. TC-8, Straße des 17. Juni 124, 10623 Berlin, Germany*
[b] *Department of Inorganic Chemistry, Fritz Haber Institute of the Max Planck Society, Faradayweg 4-6, 14195 Berlin, Germany*

Received 16 October 2006; revised 28 November 2006; accepted 28 November 2006

Abstract

Steam reforming of methanol (SRM) was investigated over copper-containing catalysts supported on four different oxides and mixed oxides: $Cu/ZnO/Al_2O_3$, $Cu/ZrO_2/CeO_2$, Cu/SiO_2, and $Cu/Cr_2O_3/Fe_2O_3$. After observing slight differences in the way of catalyst aging and experimental exclusion of mass transport limitation effects, a detailed kinetic study was carried out at 493 K. The dependence of the reaction rate on the molar ratio of methanol and water was determined, as was the influence of addition of inert nitrogen and the main reaction products hydrogen and carbon dioxide to the reactant mixture. Although there were remarkable differences in the catalytic activity of the samples, the main mechanistic steps reflected in the rate law were similar for all catalysts. The reaction rate is determined mainly by the methanol partial pressure, whereas water is not involved in the rate-determining step, except over $Cu/Cr_2O_3/Fe_2O_3$, where several differences in the chemistry were observed. Hydrogen and carbon dioxide were found to inhibit the reaction. These results were confirmed by a DRIFT study at 493 K using an equimolar reactant mixture and an excess of 4:1 of water and methanol, respectively. The same surface species could be identified on each catalyst, but neither kinetic modeling nor the DRIFT spectra could clearly indicate whether the reaction pathway occurs via a dioxomethylene species or a methyl formate species as intermediate. Similar activation energies of SRM confirm the assumption that the surface chemistry of SRM over copper-based systems is independent of the catalyst support material.

Keywords: Steam reforming of methanol; Copper catalyst; $Cu/ZnO/Al_2O_3$; $Cu/ZrO_2/CeO_2$; Cu/SiO_2; $Cu/Cr_2O_3/Fe_2O_3$; Microkinetics; Mechanistic model; DRIFTS; Surface species

1. Introduction

For environmental reasons, the replacement of combustion engines by fuel cells and electrical motors in cars is of general interest, especially in traffic-polluted metropolitan areas. The production of electricity in a H_2–O_2 fuel cell is considered a clean, energy-efficient process, producing only water as an exhaust material. The major problems are the handling, storage, and transport of hydrogen, because liquefaction is very expensive, and pressure tanks to ensure appropriate safety are suitable only for large vehicles (e.g., buses), due to their volume and weight. A very promising alternative is the physisorption on carbon nanotubes [1], but this technology is too expensive and not yet ready for technical application.

Consequently, the on-board production of hydrogen from liquid hydrogen-rich hydrocarbons has become the focus of research. Methanol was found to be a suitable candidate for on-board reforming due to a low process temperature and a high ratio of hydrogen to carbon [2]. It can be produced from fossil sources like natural gas, oil, or coal or from renewable sources like biomass [3]. Furthermore, the existing infrastructure of gas stations can also be used for methanol supply without extensive investments. A perspective on the application of methanol beyond fossil fuels has been given by Olah [4].

The steam reforming of methanol (SRM) is potentially a good process for on-board production of hydrogen for mobile fuel cells, yielding the maximum amount of hydrogen. Copper-based catalysts have been identified as outstandingly effective

* Corresponding author. Fax: +49 30 314 79552.
E-mail address: schomaecker@tu-berlin.de (R. Schomäcker).

0021-9517/$ – see front matter
doi:10.1016/j.jcat.2006.11.031

for the SRM and thus are the subject of intensive research. The formal reaction network of SRM over copper-based catalysts consists mainly of three reactions [5,6]. Steam reforming of methanol is an endothermic reaction that is as good as irreversible at temperatures above 200 °C and ambient pressure:

$$\mathrm{CH_3OH(g) + H_2O(g) \rightarrow 3H_2 + CO_2}, \quad \Delta H^0 = 49.6\ \mathrm{kJ\,mol^{-1}}. \tag{1}$$

Because this reaction is endothermic, the reactor must be heated. This is usually done by catalytic methanol combustion [7]. A less important side reaction is the decomposition of methanol (MD), which also is endothermic and nearly irreversible at temperatures above 200 °C and ambient pressure:

$$\mathrm{CH_3OH(g) \rightarrow 2H_2 + CO}, \quad \Delta H^0 = 90.6\ \mathrm{kJ\,mol^{-1}}. \tag{2}$$

The reaction products of SRM suffer the consecutive endothermic reverse water–gas shift reaction (rWGS), which is also known to be catalyzed by copper-based catalysts:

$$\mathrm{H_2 + CO_2 \rightleftharpoons H_2O(g) + CO}, \quad \Delta H^0 = 41.1\ \mathrm{kJ\,mol^{-1}}. \tag{3}$$

Although this reaction is thermodynamically strongly disfavored in the typical temperature range of SRM and due to the presence of water in the reactant mixture, it is important because it is the main reaction pathway for carbon monoxide formation [8]. The reduction of carbon monoxide, due to its poisoning effect on fuel cell electrodes, is an aim of new catalyst development with higher selectivity for SRM. Pt-based anodes are being deactivated by carbon monoxide in concentrations >20 ppm. Alternative routes, adding oxygen to the feed (combined reforming of methanol) or using a molar excess of water, lower the carbon monoxide concentration but not sufficiently to allow direct use of the product gas mixture in a fuel cell. Up to now, carbon monoxide had to be eliminated in an expensive clean-up unit, in which carbon monoxide is selectively oxidized. Additional byproducts reported by several research groups include methane, formaldehyde, dimethyl ether and methyl formate as trace components.

Concerning the reaction mechanism of SRM, a detailed model has been proposed by Peppley et al. [9] for a Cu/ZnO/Al_2O_3 catalyst. Based mainly on the extensive investigations on methanol synthesis, these authors developed expressions for the reaction rates of steam reforming of methanol (Eq. (4)), methanol decomposition, and the water–gas shift reaction. The rate expressions included surface species and intermediates that could be identified by diffuse reflectance infrared Fourier transform spectroscopy (DRIFT). For SRM, the dehydrogenation of surface methoxy groups was identified as the rate-determining step (RDS):

$$\begin{aligned} r_\mathrm{R} = {} & \left(k_\mathrm{R} K^*_{\mathrm{CH_3O^{(1)}}} \left(p_{\mathrm{CH_3OH}} / p^{1/2}_{\mathrm{H_2}}\right)\right. \\ & \times \left(1 - \left(p^3_{\mathrm{H_2}} p_{\mathrm{CO_2}} / k_\mathrm{R} p_{\mathrm{CH_3OH}} p_{\mathrm{H_2O}}\right)\right) C^\mathrm{T}_{\mathrm{S_1}} C^\mathrm{T}_{\mathrm{S_{1a}}}\Big) \\ & \Big/\Big(\left(1 + K^*_{\mathrm{CH_3O^{(1)}}} \left(p_{\mathrm{CH_3OH}} / p^{1/2}_{\mathrm{H_2}}\right)\right. \\ & + K^*_{\mathrm{HCOO^{(1)}}} p_{\mathrm{CO_2}} p^{1/2}_{\mathrm{H_2}} + K^*_{\mathrm{OH^{(1)}}} \left(p_{\mathrm{H_2O}} / p^{1/2}_{\mathrm{H_2}}\right) \\ & \left. + K^*_{\mathrm{CO^{(1)}_2}} p_{\mathrm{CO_2}}\right)\left(1 + K^{1/2}_{\mathrm{H_{(1a)}}} p^{1/2}_{\mathrm{H_2}}\right)\Big). \end{aligned} \tag{4}$$

Among the several rate expressions assembled by Lee et al. [10], this one was used directly or with slight modifications in many other studies [11–14], in most cases providing results in excellent agreement with the experimental data.

However, Peppley's comprehensive model gives no answer as to whether the reaction pathway occurs via methyl formate or dioxomethylene as an intermediate. Although the methyl formate route was predicted based on the results of Jiang et al. [15], the corresponding adsorption term was deleted in the rate expression, because methyl formate was not detectable in Peppley's DRIFT experiments. Indeed, exactly the same rate expression would be obtained assuming dioxomethylene as an intermediate and deleting its adsorption term. Because only a few research groups have detected methyl formate as trace byproduct [16–18], mostly in cases of high methanol surplus, this step of the reaction pathway remains unclear. Takezawa and Iwasa [19] and Takahashi et al. [20] have proposed a second reaction pathway via dioxomethylene through the nucleophilic addition of surface hydroxyls to adsorbed formaldehyde for a Cu/SiO_2 catalyst. This attack occurs competitively to that of methoxy groups (Fig. 1), which can explain the formation of methyl formate observed only at high MeOH/H_2O ratios.

A further assumption by Peppley is the existence of two different kinds of active sites, one for oxygenate adsorption and one for hydrogen adsorption, based on a review by Skrzypek et al. [21]. Because most of the other kinetic models found in the literature are based on a single active site, notable differences in the dependency of the reaction rate from the hydrogen partial pressure should be predicted from the rate laws, as discussed by Lee et al. [10]. Not taken into account in any model for SRM was the effect of hydrogen spillover. The existence of this elementary reaction step, although not rate-determining, was reported and proved for methanol synthesis [22,23]. Hydrogen adsorbs dissociatively on the copper surface, thereby providing a source of atomic hydrogen for methanol synthesis over oxidic phases. A possible relevancy of this process in SRM has been mentioned previously [9,24].

Up to now, only a few studies on surface species detected by DRIFT during SRM have been published. One spectrum of a Cu/ZnO/Al_2O_3 catalyst has been given by Peppley et al. [9]; another for a CuO/ZnO/ZrO_2/Al_2O_3 catalyst has been reported by Breen et al. [25]. More detailed studies on Cu/ZnO/ZrO_2 samples have been published by Matter and Ozkan [26] and Vargas et al. [27]. All of these studies reported formate and methoxy groups as the predominant surface species. Hydroxyls and formaldehyde [25] were also detected, as was gas-phase or weakly bonded carbon dioxide [9]. Neither methyl formate nor carbon monoxide was found over copper-containing catalysts

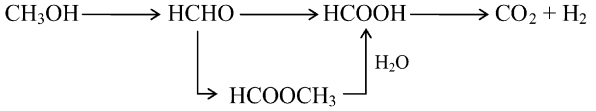

Fig. 1. Reaction pathways of steam reforming of methanol over Cu/SiO_2 catalysts proposed by Takahashi et al. [20].

in these studies. In contrast, Jacobs and Davis [3] identified carbonate and carbon monoxide in SRM over a Pt/CeO_2 catalyst, but little data are available for a comparative evaluation, because the spectra were obtained under different reaction conditions.

The present work focuses on a comparative investigation of copper-containing catalysts supported on different materials in SRM. A microkinetic study based on the differential method and supported by DRIFT spectra is presented to provide mechanistic insight into the basic reaction steps and demonstrate the influence of the support material on surface chemistry.

2. Experimental

2.1. Catalyst samples

For our experiments, we have decided to use commercial catalysts whenever possible to enable easier reproducibility of our experiments. We obtained two catalyst samples by Süd-Chemie, which were found to be active for SRM at the intended reaction conditions. One $CuO/ZnO/Al_2O_3$ low-temperature shift catalyst and one Cr_2O_3/Fe_2O_3 high-temperature shift catalyst containing a small amount of copper oxide, denoted by Süd-Chemie as C 18 HA and G-3 C, respectively, were chosen. The 6×3 mm pellets were ground and sieved to a defined particle diameter to eliminate mass transport limitation of the reaction rate.

Further $CuO/Cr_2O_3/Fe_2O_3$ catalyst samples were synthesized from metal sols, prepared from the appropriate amounts of the mixed precursors $Cu(NO_3)_2{\cdot}3H_2O$ (a Ferak product of >99.5% purity), $Cr(NO_3)_3{\cdot}9H_2O$ (Fluka, >97% purity) and $Fe(NO_3)_3{\cdot}9H_2O$ (Merck, >99% purity). The metal nitrates corresponding to 5 g of oxidic catalyst were dissolved in 300 ml of distilled water and coprecipitated as hydroxides by the addition of NaOH solution saturated with $NaHCO_3$ until the remaining solution became colorless. The coprecipitate was aged in the mother liquor overnight, then repeatedly washed with distilled water. The resulting catalyst precursor was dried (10 h at 80 °C) and calcined (3 h at 500 °C) in air, respectively.

$CuO/ZrO_2/CeO_2$ (CZC) catalysts were investigated in one of our previous kinetic studies. Detailed discussions of the preparation and characterization of these materials is available in the literature [5,28]. The CZC15 sample containing about 15 mol% CuO showed the best selectivity for SRM against CO formation, and thus it was chosen for this study.

A catalyst consisting of copper on a silica support was prepared as fourth sample by cation exchange of tetraammine copper(II) complexes [29]. A mass of 2.5 g $Cu(NO_3)_2{\cdot}3H_2O$ dissolved in 10 ml of distilled water and 10 ml of 25% ammonium hydroxide was slowly added to a stirred mixture of 5.0 g silica gel (Merck Kieselgel 100) and 30 ml of distilled water, which corresponds to a CuO content of 14.1% by weight. Because the solution became nearly colorless because of the complexation of copper on the silica surface, the deep-blue silica gel was washed several times with distilled water, then dried (for 15 h at 80 °C) and finally calcined (for 10 h at 500 °C) in air, respectively. The final copper content of this sample was determined gravimetrically after dissolution of the CuO with concentrated hydrochloric acid and repeated calcination of the colorless silica gel.

Hereinafter, the four samples $Cu/ZnO/Al_2O_3$, $Cu/Cr_2O_3/Fe_2O_3$, $Cu/ZrO_2/CeO_2$, and Cu/SiO_2 are designated as CZA, CCF, CZC, and CS, respectively. The specific surface areas of the catalyst samples were determined by nitrogen adsorption at 77 K, using a Micromeritics 2375 BET apparatus equipped with a Vacprep 061 degasser. Before acquisition of the adsorption isotherm, the samples were first outgassed at 15 Pa and 120 °C for 12 h, to ensure a clean, dry surface. The specific surface areas were calculated from the BET equation, and the average pore diameters were obtained by the BJH method from the desorption branches of the adsorption isotherms. Chemical composition data and physical properties of the catalyst samples investigated in this study are listed in Table 1.

Table 1
Characteristic data of the catalysts

	Samples (composition [% by weight])			
	CZA[a] (C 18 HA)	CCF[a] (G-3 C)	CZC[b] (CZC15)	CS
CuO	50–60	1.5–2.5	6.9	11.6
ZnO	25–35	–	–	–
Al_2O_3	8–15	–	–	–
Fe_2O_3	–	Bal.	–	–
Cr_2O_3	–	7–10	–	–
C[c]	2–3	3.5–4.5	–	–
ZrO_2	–	–	39.2	–
CeO_2	–	–	53.9	–
SiO_2	–	–	–	88.4
BET surface area [$m^2\ g^{-1}$]	68.6	74.2	102	270
Average pore diameter [nm]	16.7	12.8	9.9	15.0

[a] Composition given by suppliers data sheet.
[b] Mastalir et al. [5] reported the molar composition of CZC catalysts.
[c] Synthetic graphite.

2.2. Reactants

The liquids used in this study were methanol (Roth, HPLC grade, >99.9% purity) and distilled water. Both were degassed at 20 kPa before use. For the fine adjustment of the molar ratio of the liquid reactant mixture, an Intersmat gas chromatograph (GC) separating with a 50 m × 0.53 mm CP-Wax column at 90 °C and equipped with a thermal conductivity detector (TCD), was used. By using an exact calibration curve, surplus reactant mixture could be recycled and the production of waste liquid drastically reduced.

The gases used had the following minimum purities: N_2, 99.99%; H_2, 99.999%; and CO_2, 99.995%. They were obtained by Air Liquide.

2.3. Experimental setup

SRM was studied in a downstream fixed-bed tubular reactor (stainless steel, 10 mm i.d.). Liquid reactants were introduced by a HPLC pump (Dionex HPLC 580), and gases were dosed by a mass flow controller (MFC) into the reactor. The MFC was calibrated with nitrogen; conversion factors of 1.010 and 0.784 were used for hydrogen and carbon dioxide, respectively, calculated from the ratios of their heat capacities, c_p. Before being fed into the reactor, the methanol/water mixture and gases were preheated separately up to the desired reaction temperature. The reactor and the evaporator/preheater were surrounded by an aluminum heating block to achieve efficient heat transfer. Six cartridge heaters, 125 W each, were placed in the heating block and regulated by temperature PID control. Two thermocouples of type J (Fe/Const.) were used for temperature measurement, one located in the heating block and the other located in the catalyst bed. The catalyst was supported inside the reactor by a stainless steel grid and placed between two layers of inert Pyrex beads of the catalyst's size for better flow conditioning and heat transfer. The product mixture leaving the reactor passed two condensers at 0 and −20 °C, respectively, to remove water and methanol. The dry product gas mixture then passed a mass flow meter (MFM) calibrated with a 3:1 hydrogen/carbon dioxide mixture for conversion measurement. The condensed liquid was analyzed with the Intersmat GC described in Section 2.2 to detect byproducts such as methyl formate or dimethyl ether. The composition of the dry product gas was monitored with a Varian 3800 GC also equipped with a TCD. Helium was applied as a carrier gas, and separation was achieved with a 25 m × 0.53 mm CarboPLOT P7 column at 31 °C.

2.4. Catalytic measurements

First, mass transport limitation effects were quantified for CZA, by far the most active catalyst in this study. Here 0.5 g of sieved particle size fractions from 100–200, 200–300, and 300–450 µm of the catalyst were placed into the reactor and fed with a 0.3 ml min^{-1} equimolar methanol/water mixture at 220 °C. The initial conversion after a 30-min reduction period could be calculated from the measured product gas flow rate.

Table 2
Charges of catalyst and copper during the kinetic measurements

Sample	CZA	CCF	CZC	CS
Catalyst mass [g]	0.5	2.5	1.0	2.0
Included mass of copper [g]	0.250–0.300	0.038–0.063	0.069	0.232
Particle size [µm]	200–300	200–300	100–300	63–200

Catalytic measurements started with a reduction period of 15 h at 220 °C with a feed of 10 ml$_n$ min^{-1} of hydrogen followed by 0.05 ml min^{-1} of an equimolar methanol/water mixture. The amounts and particle sizes of each catalyst for kinetic measurements are given in Table 2.

After catalyst aging, which took at least several days, kinetic measurements were conducted. The molar ratio of the reactants was varied with and without addition of nitrogen, hydrogen, and carbon dioxide as follows:

- CH_3OH/H_2O molar ratio from 1:9 to 9.5:1,
- N_2 and H_2 addition from 20 to 80%,
- CO_2 addition from 20 to 60%.

To keep the conversion of the minor component below 10%, the liquid flow rate was adjusted between 0.05 and 0.5 ml min^{-1}, and gases were added at a flow rate of 50–250 ml$_n$ min^{-1}. The molar ratios were changed not systematically (e.g., increasing water content), but rather randomly, to avoid tendencies originating from the experimental process or misinterpretation of catalyst aging effects. However, the gases were added to the given CH_3OH/H_2O composition in increasing concentrations (20/40/60/80%) in the order N_2, H_2, CO_2.

2.5. DRIFTS experiments

In situ DRIFTS was conducted using the Graseby Specac Diffuse Reflectance Optics "Selector" and "Environmental Cell" (zinc selenide window). This unit operates with a Bruker IFS 66 FTIR spectrometer equipped with a mercury cadmium telluride (MCT) detector. Both reactants were dosed via saturators (water: 30 °C; methanol: 4 °C) in a helium stream. Their concentrations in the combined stream were controlled via the adjustment of three mass flow controllers ($He_{sat,methanol}$, $He_{sat,water}$, and He), with calculations based on the Antoine equation [30]. The overall reactant concentration was 4% in a total flow of 10–15 ml min^{-1}. The sample holder was filled with 15–50 mg of the <25 µm catalyst powder, depending on its density. Each catalyst was reduced for 2 h in a 4% methanol flow at 250 °C, then cooled to 220 °C and kept in the methanol flow overnight to remove the high amount of adsorbed water on the catalyst surface via SRM reaction and achieve steady-state conditions. DRIFTS measurements were conducted beginning at a 4:1 methanol excess and decreasing methanol-to-water ratio. The reaction products were analyzed on-line by MS (Pfeiffer Omnistar). DRIFT spectra were collected after steady-state conditions were achieved. Typically, 1000 scans were averaged at a resolution of 4 cm^{-1}, due to a low signal-to-noise ratio of the reduced copper catalysts. The single-channel sample spectra were divided by a KBr background spectrum, obtained before

in situ measurements. The resulting spectra were transformed into the Kubelka–Munk function.

3. Results and discussion

3.1. Mass transport limitation

For microkinetic modeling, it is important to eliminate any mass transport limitations on the reaction rate. Several authors have reported diffusion limitations in SRM over $Cu/ZnO/Al_2O_3$ catalysts. In a previous study on a different commercial catalyst (Süd-Chemie MeOH1), a reduced reaction rate was observed at a particle size of 0.71–1.00 mm [8] and temperature of 250 °C. Lee et al. [10] predicted mass transport limitations at 240 °C for their catalyst (Synetix 33-5) from theoretical calculations; however, besides the larger particle diameter in both of the studies, their catalysts were about three to five times more active than the $Cu/ZnO/Al_2O_3$ catalyst investigated in the present study, which may explain their results. In contrast, Jiang et al. [31] found no dependence of particle diameter of 150–190 μm on the reaction rate in their studies using commercial catalysts (BASF S3-85), even though they used a more active catalyst and worked at temperatures of 160–260 °C. This result was also reported by Peppley et al. [6], investigating SRM over a $Cu/ZnO/Al_2O_3$ catalyst (BASF K3-110) with a particle size of 710–850 μm in the same temperature range.

We applied the Weisz–Prater criterion using the Weisz modulus Ψ' as dimensionless quantity to estimate diffusion limitations [32] and confirmed our results with experimental determination of the influence of pore diffusion for the most active catalyst, CZA. The Weisz modulus, which gives the ratio of the reaction rate to the diffusion rate in a porous catalyst pellet, is

$$\Psi' = L^2 \frac{m+1}{2} \frac{r_{\text{eff}} \rho_{\text{cat}}}{D_{\text{eff,M}} c_{\text{M}}}, \tag{5}$$

where L is the characteristic length (m) given by one-third of the particle radius for spherical particles, m is the reaction order of methanol, r_{eff} is the measured reaction rate (mol s^{-1} kg^{-1}), ρ_{cat} is the catalyst density (kg m^{-3}), $D_{\text{eff,M}}$ is the effective diffusivity of methanol (m^2 s^{-1}), and c_{M} is the gas phase concentration of methanol at the catalyst surface (mol m^{-3}). At ambient pressure, the diffusivity in porous solids is reduced to Knudsen diffusivity at pore diameters <100 nm. With a typical tortuosity value of $\tau = 3.5$ [33] and a measured porosity of $\varepsilon = 0.7$, we determined the effective Knudsen diffusivity of methanol to be $D_{\text{K,eff,M}} = 6.4 \times 10^{-7}$ m^2 s^{-1}. Because a reaction order of 0.5 for methanol results in Weisz moduli of $\Psi' \ll 1$ for the chosen particle size fraction, the Weisz–Prater criterion predicts no mass transport limitation for our reaction conditions and an effectiveness factor of $\eta \approx 1$.

This theoretical result was confirmed by experimental tests. No change in reaction rate was observed when varying the particle diameter of CZA in the range of 100–450 μm, indicating no mass transport limitation at 220 °C. Our previous study found only insignificant mass transport limitation in CZC [5]. Using a small particle size fraction of 100–300 μm, an affect on reaction rate was excluded. Because the most active catalysts proved to be gradientless under the chosen reaction conditions, similar tests with CCF and CS were omitted because of lower activity, similar pore diameter, smaller particle size (for CS), and very low copper content (for CCF).

3.2. Catalyst aging

It is well known that copper catalysts used in methanol synthesis and in SRM deactivate rapidly during the initial period of operation. Irreversible alloy formation of the active copper species with support material and thermal sintering of small Cu particles, and thereby the reduction of the active surface area, are two possible reasons for this effect [34,35]. Zhang and Shi [36] reported a positive effect of ceria on the preservation of high copper dispersion and consequently enhanced long-term stability. The same effect was found by Szizybalski et al. [37] using zirconia as a support material. Another factor is the deposition of coke on the catalyst surface. Liu et al. [18] removed up to 1.7 wt% of coke from their Cu/CeO_2 catalyst by recalcination in air and again reached the initial activity. Coke formation was observed by XPS and even fitted with a kinetic model for a $Cu/ZnO/Al_2O_3$ catalyst by Agarwal et al. [38]. As a fourth reason, a change in the oxidation state of copper from Cu(II) to Cu(0) was found to be responsible for catalyst deactivation by Choi and Stenger [17], who observed copper reduction with XPS during the first 100 h of operation of their $Cu/ZnO/Al_2O_3$ catalyst.

Because kinetic measurements took about 1 week for each catalyst, a change in catalyst activity during this time period had to be excluded. Therefore, the catalysts were aged for several days under identical reaction conditions until they reached constant conversion in SRM. The deactivation of the samples after the reduction period is presented in Fig. 2. This figure clearly shows that each catalyst lost about 30–40% of its initial activity after 100 h time on stream. Whereas CZA, CCF, and CZC reached a constant activity, CS seemed to deactivate and to not be a stable catalyst under SRM conditions. Concerning CZC,

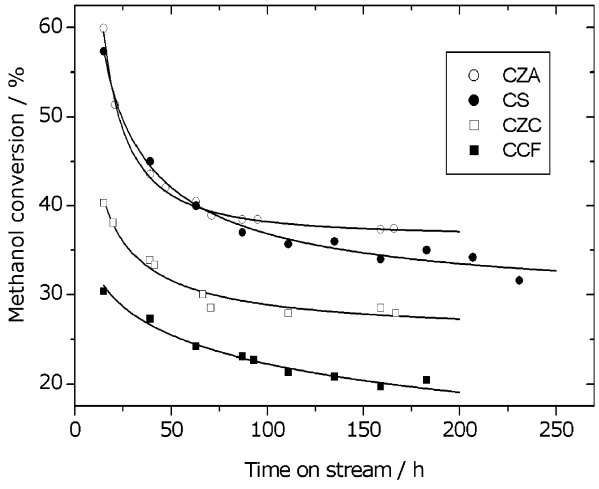

Fig. 2. Initial catalyst deactivation of copper catalysts during SRM as a function of time on stream ($m_{\text{CZA}} = 0.5$ g, $m_{\text{CCF}} = 2.5$ g, $m_{\text{CZC}} = 1.0$ g, $m_{\text{CS}} = 2.0$ g, $T = 220$ °C, $p = 1$ bar, $w = 0.05$ ml min^{-1}, $MeOH/H_2O = 1$).

it is interesting that deactivation stopped earlier and the catalyst maintained a comparatively higher activity at 220 °C than at 250 °C [5]; at the latter temperature, this catalyst lost more than half of its initial activity and became stable after 200 h on stream. This result is in agreement with the observation of thermal sintering of the copper particles during SRM conditions, especially at higher temperatures.

3.3. DRIFTS experiments

A series of DRIFT spectra were collected to obtain information about the surface reactions and intermediates during SRM. Based on previous studies [9,25–27] and the proposed mechanism over $Cu/ZnO/Al_2O_3$ catalysts, the appearance of hydroxyl, methoxy, and formate groups was expected, as was carbon dioxide as gas-phase or weakly bonded surface species. One aim of this study was to determine whether the reaction occurs mainly via dioxomethylene or via methyl formate by detecting one of these species on the catalyst surface. The reactant composition was varied from methanol excess to water excess in an effort to observe a dependence of the band areas on the reactant partial pressure and thereby support the mechanistic model as a basis for the kinetic model.

The process of DRIFT spectra conversion and manipulation is shown in Fig. 3 for CZA and a feed composition of $MeOH/H_2O = 1{:}1$. The raw data of the DRIFT spectra from the catalyst before feed addition (a) and in situ during SRM reaction (b) were both Kubelka–Munk transformed into spectra (c) and (d), respectively. As can be seen from the strongly different intensity, a simple subtraction of these spectra would result in negative bands; thus, spectrum (c) was weighted with the factor 0.35 before being subtracted from spectrum (d). The weighting factors were determined individually, using the carbonate band at 1350–1500 cm^{-1} for orientation. Finally, the resulting difference spectrum (e) was baseline-adjusted (f) for clarity and comparability, as necessary.

The DRIFT spectrum of CZA was of relatively low quality, which may be ascribed to the high copper content of this catalyst. Peppley et al. [9] also reported a spectrum of a high-Cu content $Cu/ZnO/Al_2O_3$ catalyst, with comparatively high signal-to-noise ratio. The reflectance, which was >10% in a wide spectral range for the oxidized catalyst, sustained a drastic drop during the reduction period (see also Fig. 3 (a) and (b)), and the resulting spectra allow only cautious statements about the absence of surface intermediates. A dilution of the catalyst with inert α-alumina powder had no effect on the signal-to-noise ratio. Vargas et al. [27] also observed decreased intensity over a reduced $Cu/ZnO/Al_2O_3$ catalyst compared with the oxidized sample.

As can be seen from Fig. 4, the same intermediates were found on each investigated copper-based catalyst. Surface hydroxyls were present on the surface of all catalysts but CCF, with broad features at 3000–3800 cm^{-1}. Also identified on every surface was the characteristic pattern of two methoxy bands bordering one formate band at 2800–3000 cm^{-1} from C–H stretching modes. The bands at around 2349 cm^{-1} can be attributed to the two branches of the rotation vibration spectrum

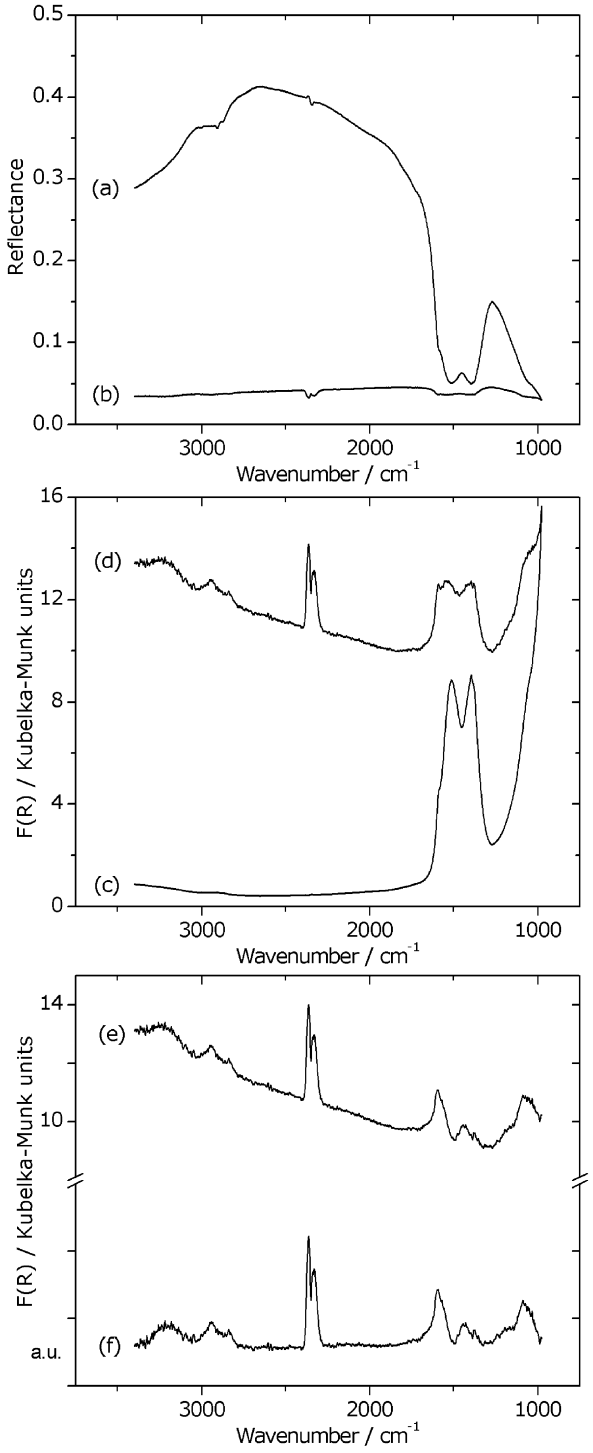

Fig. 3. Process of DRIFT spectra editing prior to presentation, exemplarily shown for CZA with a feed composition of $MeOH/H_2O = 1{:}1$.

of gaseous carbon dioxide. Surface copper carbonyls were observed only on CZC and CS, with a feature at 2092 cm^{-1}. Surprisingly, no CO was detected on the surface of CCF, although this catalyst demonstrated the worst selectivity in the on-line analysis based on the DRIFTS measurements as well as in the kinetic measurements. The region at 1000–1600 cm^{-1} contained bands of carbonates, as well as features from methoxy and formate C–O stretching and C–H bending modes. These

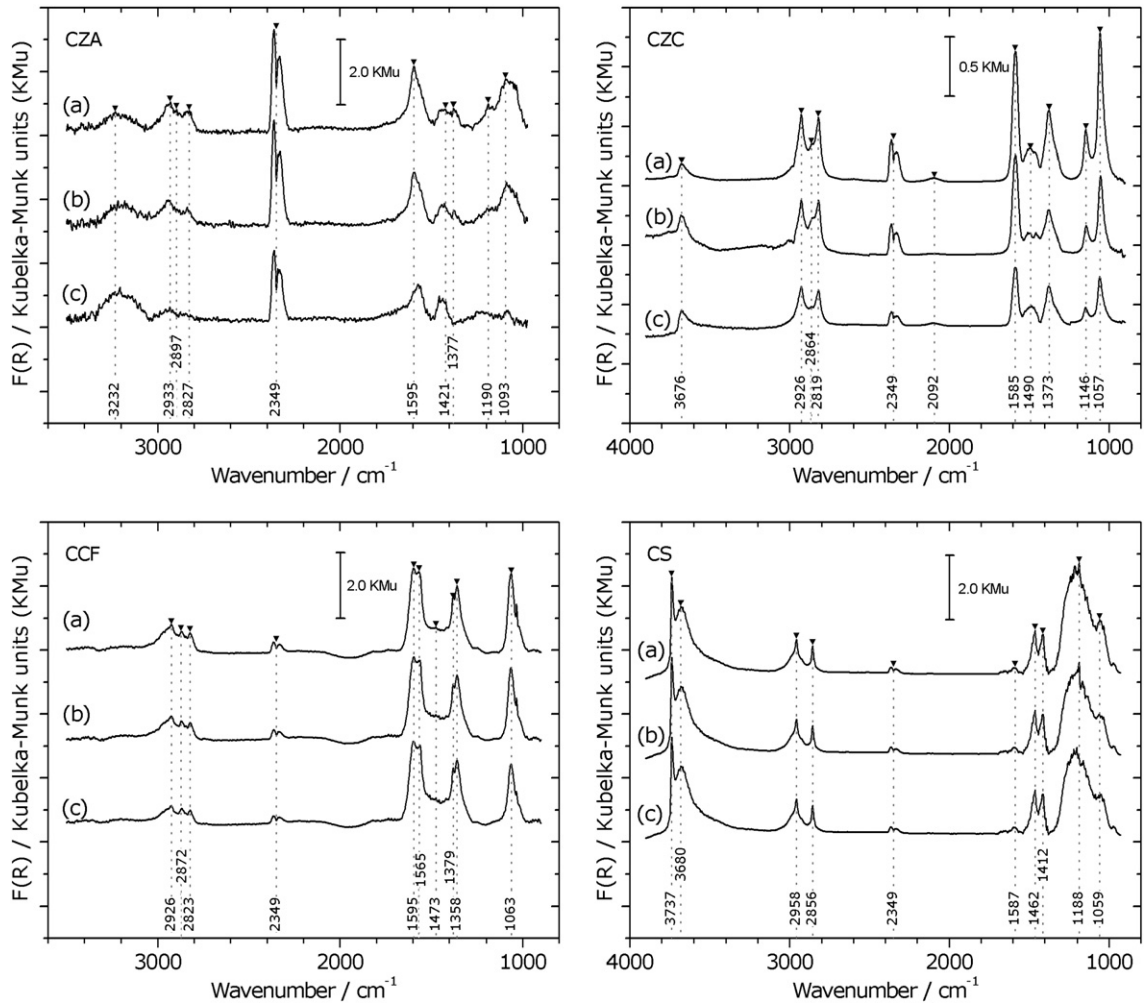

Fig. 4. DRIFT spectra of the investigated catalysts CZA, CCF, CZC, and CS, collected at 220 °C, reactant overall concentration 4% in helium. (a) $MeOH/H_2O$ = 4:1, (b) $MeOH/H_2O$ = 1:1, (c) $MeOH/H_2O$ = 1:4, respectively.

bands are summarized and assigned to surface species and their vibrational modes (along with the references for these assignments) in Table 3.

Over CCF, the asymmetric OCO stretching band and the CH bending band of formate species appeared to be divided into two neighboring bands at 1358/1379 and 1565/1595 cm^{-1}. This can indicate either monodentate and bidentate formate adsorption [39] or the parallel adsorption of formate on two different kinds of surfaces [27] that may be present in the CCF catalyst. On the other hand, a shoulder at about 1360 cm^{-1} was also seen on CZC. This feature, as well as the band at 1358 cm^{-1} on CCF, also may be attributed to symmetric OCO stretching.

These spectra also can be evaluated semiquantitatively. Except for CS, the DRIFT spectra of which seem to be independent of the feed composition, the band areas of methoxy groups clearly increased with increasing methanol partial pressure. In contrast, the intensity of surface hydroxyls decreased because the overall concentration of the reactants was kept constant at 4%. Integration of the hydroxyl bands (3232 and 3676 cm^{-1} for CZA and CZC, respectively) and the bands of methoxy groups (1093, 1057, and 1063 cm^{-1} for CZA, CZC, and CCF, respectively) after fitting resulted in good linear correlations of the band areas with the methanol (methoxy groups) and water (hydroxyl groups) partial pressure in the feed. This confirms the appearance of the corresponding adsorption terms in the mechanistic rate equation from independent spectroscopic experiments. As expected, the signal of the gas-phase carbon dioxide correlated with the measured conversion in this experimental series and was stronger with higher methanol partial pressure. The latter indicates that the reaction rate depends more on the methanol than on water partial pressure, because other reaction parameters (e.g., temperature, contact time) were kept constant during this experimental series. However, bands of methyl formate, expected at 1666 and 1726 cm^{-1} [40], which was detected by MS only over CS in traces and only in the case of high methanol surplus in the feed, or dioxomethylene, expected at 1405 and 2765 cm^{-1} [39], were absent, as were bands of formaldehyde, expected at 1148 cm^{-1} [26], another "missing" intermediate in the assumed reaction pathway. It appears that these species either do not participate in the SRM reaction mechanism or transform too rapidly to enable detection with infrared spectroscopy; consequently, this part of the reaction network cannot be clarified using this technique.

Table 3
Observed bands from the DRIFT spectra of SRM over the reduced Cu catalysts and assignment to vibrational modes of surface species and gas phase species (indicated as such)

Species	Mode[a]	CZA	CCF	CZC	CS	$Cu/ZnO/ZrO_2$	$Cu/ZnO/Al_2O_3$	Fe_2O_3/SiO_2	Pt/CeO_2	Cu/SiO_2	
						[26]	[27]	[52]	[3]	[40]	[39]
Methoxy	$\nu(CH)_a$	2933	2926	2926	2958	2926	2950		2920	2960	2951
	$\nu(CH)_s$	2827	2823	2819	2856	2821	2830		2820	2859	2851
	$\delta(CH)_a$				1462			1466 1438		1463	
	$\rho(CH_3)$	1190		1146	(1188)		1190				
	$\nu(CO)$	1093	1063	1057	1059	1047	1081		1080		
Hydroxy	$\nu(OH)$				3737		3735			3738	
	$\nu(OH\cdots O)$	3232		3676	3680		3445		3650	3650	
Formate	$\nu(CH)$	2897	2872	2864		2871	2896		2830		2902
	$\nu(OCO)_a$	1595	1595 1565	1585	1587	1600	1594 1610	1567	1580		1564
	$\delta(CH)$	1377	1379 1358	1373		1357	1390	1377	1350		
Gas phase or weakly adsorbed carbon dioxide						2359 2327					
Gas phase carbon dioxide		2349	2349	2349	2349		2341				
Carbonyls				2092		2095					
Carbonate		1421		1490	1412		1550 1395		1460		1415

[a] ν: stretch; δ: bend; ρ: rock.

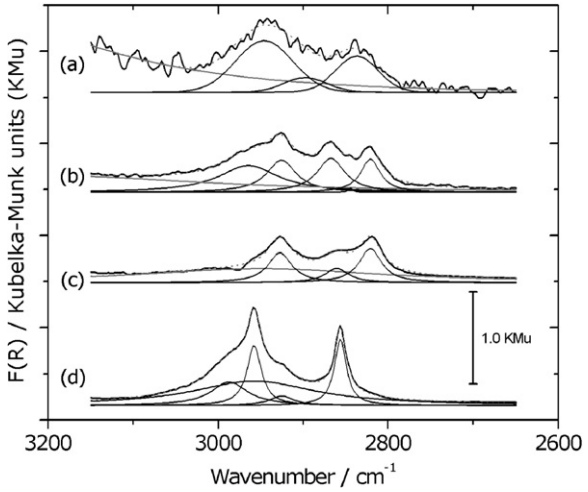

Fig. 5. Fit of spectra (b) of each catalyst from Fig. 3; (a) CZA, (b) CCF, (c) CZC, (d) CS; feed: 4% reactants ($MeOH/H_2O = 1{:}1$), 220 °C.

Another observation concerning the range of 2600–3200 cm^{-1} is the signal of the formate group, which was comparatively strong on CCF and nearly invisible on the other three catalysts. Because the absolute band area is not meaningful in itself without knowledge of the extinction coefficients, the ratio of the band areas from the symmetric ν(CH) bands of the formate groups and the methoxy groups was calculated from the fits of the spectra; these values are given in Fig. 5 and Table 4. Note that the wavenumbers given in the table result from the fits and may differ slightly from the values shown in Fig. 5.

Table 4
Band areas and ratios of the $\nu(CH)_s$ bands of the formate and the methoxy groups

Catalyst	$\nu(CH)_s$ methoxy	Band area	$\nu(CH)_s$ formate	Band area	Ratio
CZA	2836	24.7	2897	10.1	2.5
CCF	2820	15.8	2867	23.2	0.7
CZC	2821	18.8	2860	8.3	2.3
CS	2855	19.4	2925	5.6	3.5

These ratios clearly indicate that the surface of CCF is relatively heavily covered with formate groups compared with that of the other catalysts. This means that formate groups on this catalyst are relatively stable, and their decomposition by dehydrogenation may have an affect on the overall reaction rate. Along with the results of the kinetic model discrimination (which are discussed in more detail later), these findings confirm the difference in the RDS of SRM over $Cu/Cr_2O_3/Fe_2O_3$ compared with already well-investigated $Cu/ZnO/Al_2O_3$ and Cu/SiO_2 systems.

Further information from the fits included the presence of another methoxy-related band at 2987 cm^{-1} on CS and 2964 cm^{-1} on CCF. These bands, not observed on CZA and CZC, also may be attributed to C–H stretching vibrations.

3.4. Kinetic modeling

3.4.1. Contact time

For kinetic modeling, knowledge of the contact time is an essential condition. Determining contact time may be difficult,

especially for isobaric gas-phase reactions with expanding or contracting volume due to a change in the total mole number. Measurements in the high-conversion regime require numerical integration, because the resulting deviation is dependent on the conversion and will cause a systematic error. This may be irrelevant for kinetics developed for technical application, but for mechanistic studies, the determination of contact time merits at least as much attention as the analysis of the product mixture. In our case, we measured mainly differential conversions of <10%, so conversion can be considered directly proportional to contact time. We also had to consider the molar ratio λ of the reactants and added gases such as N_2, H_2, and CO_2. Measuring in the linear range, the contact time can be calculated from

$$\tau = \frac{V_R}{\dot{V}_0}\frac{1}{BX}\ln\left(\frac{A+B+BX}{A+B}\right), \tag{6}$$

where V_R is the catalyst bed volume (m^3), $\dot{V}_0$ is the initial gas flow rate ($m^3\,s^{-1}$), and X is the conversion of the reactant present as a minor component. The coefficients A and B depend on the molar ratio of methanol and water, $\lambda = n_{MeOH}/n_{H_2O}$, and are given by

	A	B
$\lambda \leqslant 1$	$x_{gas,0} + (1 - x_{gas,0})(1-\lambda)/(1+\lambda)$	$(1 - x_{gas,0})2\lambda/(1+\lambda)$
$\lambda \geqslant 1$	$x_{gas,0} - (1 - x_{gas,0})(1-\lambda)/(1+\lambda)$	$(1 - x_{gas,0})2/(1+\lambda)$

where $x_{gas,0}$ is the initial molar ratio of added gas. Fig. 6 shows the deviation of the contact time with increasing conversion in SRM calculated from Eq. (6) and from numerical integration as done in our previous work [5].

The most accurate calculation is of course the numerical integration (model 3), but, as can be seen from Fig. 6, model 2 (Eq. (6)) reaches close approximation to the "real" contact time up to a conversion of 20%. In contrast, neglecting the increase in volume (model 1), the deviation is about 5% at a conversion of 10%.

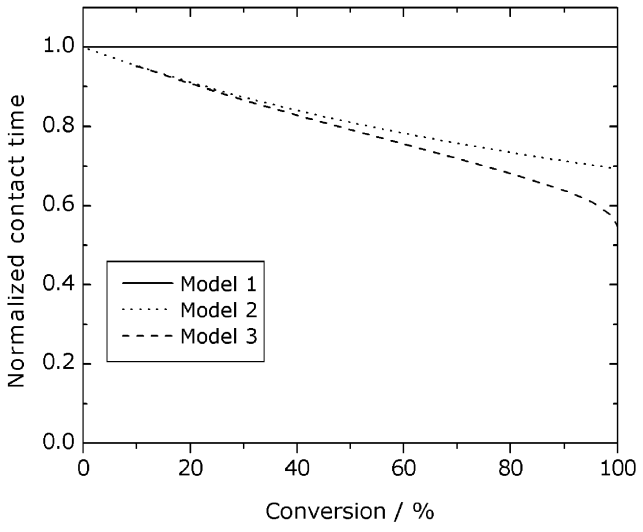

Fig. 6. Predicted reduction of the contact time during SRM as a function of conversion due to increase of total mole number, calculations for equimolar reactant mixture. Model 1: contact time related to initial flow rate (no change in mole number, full line); model 2: contact time calculated from Eq. (6) (short dashed line); model 3: contact time from numerical integration [5] (long dashed line).

3.4.2. Microkinetic model

The development of a possible microkinetic model for SRM over a commercial $Cu/ZnO/Al_2O_3$ catalyst has been described in detail by Peppley et al. [9]. Because most of our experimental data can be explained using this proposed reaction mechanism, it was taken as basis of our investigations. The catalytic cycle begins with the dissociative adsorption of methanol on the catalyst surface, which is assumed to include two distinct types of active sites: one responsible for hydrogen adsorption (type 1a) and the other responsible for the adsorption of all other intermediates (type 1), which are exclusively oxygen-bonded. In this study, the adsorption sites are designated type A and type B instead of 1 and 1a, respectively. Jung and Bell [23], in their study of methanol synthesis, assigned the adsorption of hydrogen to the metallic copper surface, whereas the oxygenate chemistry occurs on the ceramic support (in this case, ZrO_2). A similar assignment in case of SRM is possible due to the microreversibility principle. Matter and Ozkan [26] proposed methanol adsorption over hydroxylated surfaces via water formation. From our experiments, this cannot be excluded, because at the end a similar reaction rate law would result. However, a methoxy group exhibiting dehydrogenation as the RDS of the overall reaction was also found by Lee et al. [10] and Jiang et al. [31] in their kinetic studies. The formaldehyde thus formed is immediately attacked by a methoxy group, resulting in the intermediate methyl formate [41,42], which was observed in several SRM studies as a byproduct in trace amounts, exclusively in the case of methanol surplus in the reactant mixture. One other reaction pathway toward methyl formate is described by the reaction of methanol with formate groups, as identified by Busca et al. [43] over VO_x/TiO_2 catalysts during methanol decomposition and partial oxidation. This reaction pathway appears less feasible over partly reduced copper catalysts due to the limited (and doubtful) ability to assign kinetic data from these greatly different catalyst systems and reaction conditions. However, methyl formate decomposes when in contact with hydroxyl groups to methoxy and formate groups. One other reaction mechanism was given by Takezawa and Takahashi et al. [19,20], who proposed the attack of formaldehyde by surface hydroxyls, resulting in the formation of dioxomethylene as a reaction intermediate. Dioxomethylene, the intermediate of the reverse methanol synthesis reaction, is supposed to dehydrogenate into a formate group. However, neither methyl formate nor dioxomethylene was observed in the DRIFTS study and thus will not appear in the adsorption term of the microkinetic rate law, which in this case then appears identical for both reaction mechanisms. The formate group dehydrogenates again to release carbon dioxide from the type A surface; the accumulated hydrogen desorbs molecularly from the type B surface.

The entire catalysis cycle of SRM is given schematically in Fig. 7. Adopting the Hougen–Watson formalism, based on the Langmuir adsorption isotherms, the kinetics of this catalysis cycle can be formulated using the following assumptions:

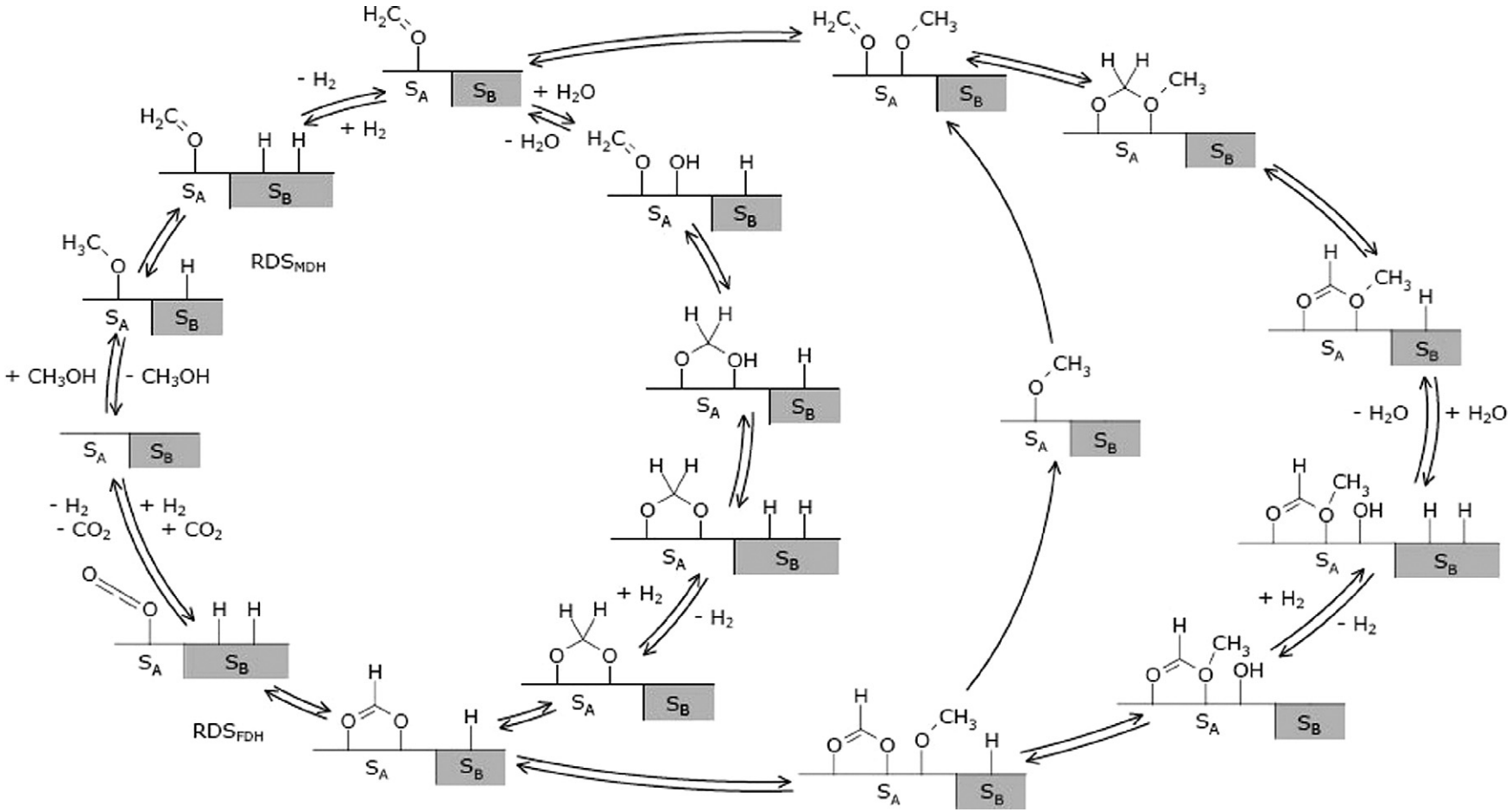

Fig. 7. Catalysis cycle of methanol steam reforming on the basis of the investigations of Jiang at al. [15], Peppley et al. [9] and Takezawa and Iwasa [19], including different kinds of reactive surface sites A (□) and B (■).

(1) The dehydrogenation of the methoxy group is the RDS; all of the other elemental reactions are in thermodynamic equilibrium.
(2) Oxygenates adsorb competitively and mostly in one monolayer on surface A, whereas hydrogen adsorbs dissociatively on surface B.
(3) Only adsorbates observed in the DRIFTS study are considered in the adsorption term; in addition, the adsorption of carbon dioxide is taken into account.
(4) Measuring in the low-conversion regime, the reverse reaction is negligible.

The microkinetic rate equation of SRM is then given by the following equation, in which the index MDH means methoxy dehydrogenation:

$$\begin{aligned} r_{\mathrm{MDH}} &= -\frac{\partial p_{\mathrm{MeOH}}}{\partial t} = k_{\mathrm{MDH}} c_{\mathrm{CH_3O^{(A)}}} c_{\mathrm{(B)}} \\ &= \left(k_{\mathrm{MDH}} C^{\mathrm{T}}_{\mathrm{S_A}} C^{\mathrm{T}}_{\mathrm{S_B}} K^{*}_{\mathrm{CH_3O^{(A)}}} \left(p_{\mathrm{CH_3OH}} / p^{1/2}_{\mathrm{H_2}}\right)\right) \\ &\quad \Big/ \Big(\Big(1 + \underbrace{K^{*}_{\mathrm{CH_3O^{(A)}}} \left(p_{\mathrm{CH_3OH}} / p^{1/2}_{\mathrm{H_2}}\right)}_{\text{methoxy}} \\ &\quad + \underbrace{K^{*}_{\mathrm{OH^{(A)}}} \left(p_{\mathrm{H_2O}} / p^{1/2}_{\mathrm{H_2}}\right)}_{\text{hydroxy}} + \underbrace{K^{*}_{\mathrm{HCOO^{(A)}}} p_{\mathrm{CO_2}} p^{1/2}_{\mathrm{H_2}}}_{\text{formate}} \\ &\quad + \underbrace{K_{\mathrm{CO_2^{(A)}}} p_{\mathrm{CO_2}}}_{\text{carbon dioxide}}\Big)\left(1 + K^{1/2}_{\mathrm{H^{(B)}}} p^{1/2}_{\mathrm{H_2}}\right)\Big). \end{aligned} \tag{7}$$

Here k_{MDH} is the rate constant and $C^{\mathrm{T}}_{\mathrm{S_A}}$ and $C^{\mathrm{T}}_{\mathrm{S_B}}$ are the total concentrations of type A and type B adsorption sites, respectively. Because these three values cannot be determined individually by parameter fitting, their product k^* was taken for this process:

$$k^* = k_{\mathrm{MDH}} C^{\mathrm{T}}_{\mathrm{S_A}} C^{\mathrm{T}}_{\mathrm{S_B}}. \tag{8}$$

The combined adsorption constants K^* given in the adsorption term are defined as

$$K^{*}_{\mathrm{CH_3O^{(A)}}} = \frac{K_{\mathrm{CH_3OH^{(A,B)}}}}{K^{1/2}_{\mathrm{H_2^{(B)}}}}, \tag{9}$$

$$K^{*}_{\mathrm{HCOO^{(A)}}} = \frac{K_{\mathrm{CO_2^{(A)}}} K^{1/2}_{\mathrm{H_2^{(B)}}}}{K_{\mathrm{HCOO^{(A,B)}}}}, \tag{10}$$

and

$$K^{*}_{\mathrm{OH^{(A)}}} = \frac{K_{\mathrm{H_2O^{(A,B)}}}}{K^{1/2}_{\mathrm{H_2^{(B)}}}}, \tag{11}$$

with the temperature dependence of rate and adsorption constants given by the Arrhenius (Eq. (12)) and van't Hoff (Eq. (13)) equations, respectively:

$$k = k_0 e^{-E_{\mathrm{A}}/(RT)} \tag{12}$$

and

$$K = K_0 e^{-\Delta H_{\mathrm{ads}}/(RT)}. \tag{13}$$

Equation (7) predicts a SRM reaction rate that is determined mainly by the partial pressure of methanol. For water, the rate shows a weak reverse dependence, expressed by a negative reaction order in a power law approach. The adsorption of carbon dioxide is competitive to that of methanol, water, and the oxygenate intermediates and thereby inhibits the overall reaction. Moreover, water and methanol adsorption occur dissociatively in combination with dehydrogenation, which should lead to strong inhibition by hydrogen. These predictions from the mechanistic rate law were compared with the experimental data. Because the kinetic measurements were conducted under isothermal conditions at 220 °C, values for activation energy, E_{A}, and heat of adsorption ΔH_{ads}, could not be determined, except an apparent activation energy for the overall rate, as discussed in Section 3.5.

For each catalyst, the rate constant, as well as the adsorption constants of methanol, water, hydrogen, and carbon dioxide and the equilibrium constant of formate formation on the surface given in Eq. (7), were fitted to a total set of approximately 150 experimental rate data, calculated in the low-conversion regime from the ratio of methanol conversion and contact time. The multiparameter fit was optimized by minimization of the mean squared error (MMSE). The following rate and adsorption constants of SRM over the catalysts CZA, CZC, and CS were determined (Table 5) at a reaction temperature of 220 °C. Because CCF showed a particularly different catalytic behavior than the other three catalysts and could not be fitted with the model described above, its modeling is described later.

Table 5
Parameters of microkinetic modeling of SRM over supported copper catalysts CZA, CZC, and CS, given with confidence interval (±5% of the absolute rate value) and stability index R^2

	CZA	CZC	CS	K3-110 [9]	Synetix 33-5 [10]
k^* [bar s^{-1}]	0.537 ± 0.008	0.422 ± 0.012	0.0920 ± 0.003		
$K^*_{\mathrm{CH_3O^{(A)}}}$ [bar$^{-0.5}$]	1.16 ± 0.06	0.86 ± 0.06	1.02 ± 0.08	0.862	4.93
$K^*_{\mathrm{OH^{(A)}}}$ [bar$^{-0.5}$]	0.06 ± 0.01	0.035 ± 0.015	0.033 ± 0.017	0.623	–
$K^*_{\mathrm{HCOO^{(A)}}}$ [bar$^{-1.5}$]	17 ± 4	6.71 ± 0.18	7.4 ± 0.6	0.058	–
$K_{\mathrm{CO_2^{(A)}}}$ [bar^{-1}]	0.65 ± 0.07	7.2 ± 0.6	3.8 ± 0.4	–	–
$K_{\mathrm{H_2^{(B)}}}$ [bar^{-1}]	0.41 ± 0.09	0.77 ± 0.02	0.288 ± 0.011	1.16	12.6
R^2 (see Fig. 8)	0.992	0.989	0.988		

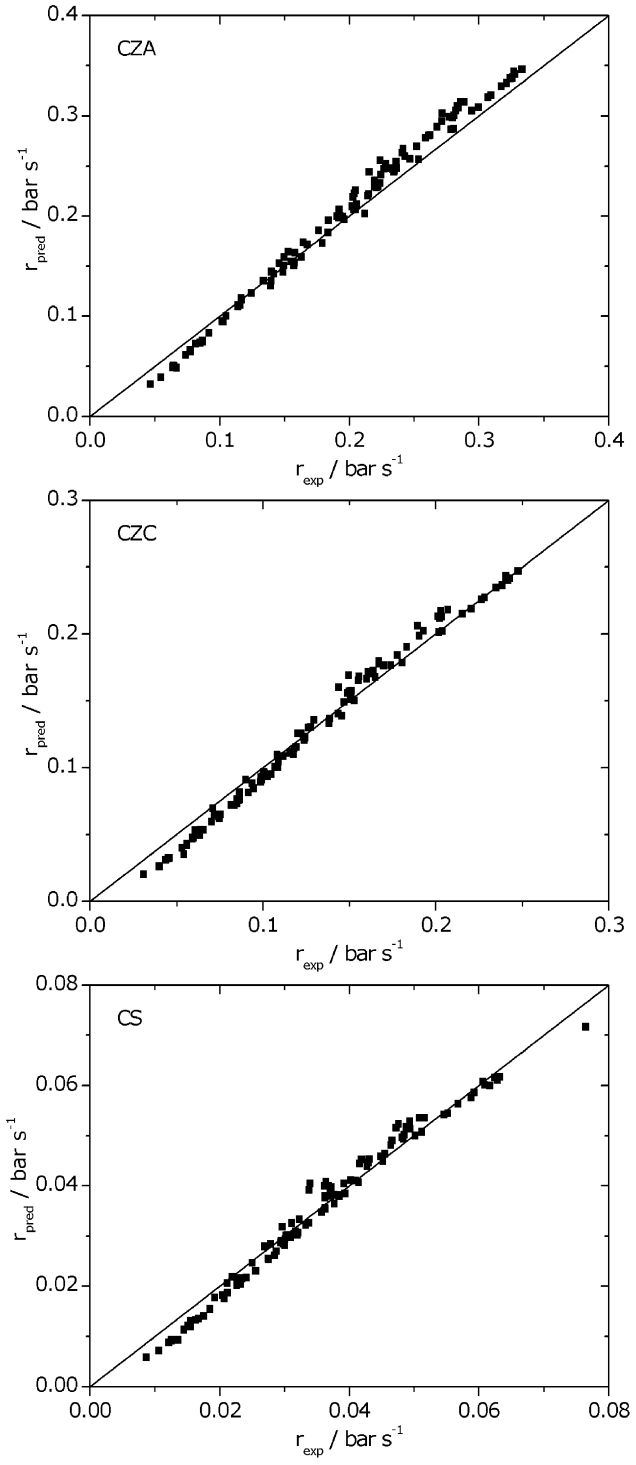

Fig. 8. Parity plots of microkinetic modeling of SRM over CZA, CZC, and CS.

As can be seen from the confidence intervals, the rate constant k^* was determined with the highest accuracy, whereas the adsorption constants $K^*_{CH_3O^{(A)}}$, $K^*_{OH^{(A)}}$, and $K_{H_2^{(B)}}$ could be fitted only with moderate exactness. Because $K_{CO_2^{(A)}}$ and $K^*_{HCOO^{(A)}}$ affect each other in the prediction of the surface inhibition caused by carbon dioxide, by either molecular adsorption or formate formation, their values have a relatively low accuracy. This also may explain the difference in the ratio of $K^*_{HCOO^{(A)}}$ and $K_{CO_2^{(A)}}$ regarding CZA on the one hand and CZC and CS on the other hand. Nevertheless, the elimination of one of these constants resulted in a significant loss of fitting quality, and so both of them were kept in the rate equation. However, the stability index R^2 is between 0.95 and 1.0 for the three catalysts, confirming the good agreement between the experimental data and the microkinetic model. To provide a better comparison of the rate constants and to obtain information about the intrinsic rate constants, the k^* values must be referred to the number of active sites on the catalyst surface. These surface concentrations are, of course, dependent on the copper content of the samples, but certainly are not linear functions due to agglomeration effects related to higher copper content. However, because the absolute number of active sites remains unknown, a relatively rough comparison of the reaction rates related to the copper content is given in Section 3.5. Compared with previously published data, the fitted parameters $K^*_{CH_3O^{(A)}}$ and $K_{H_2^{(B)}}$ for CZA come closer to the corresponding constants that Peppley et al. [9] determined than to the adsorption constants that Lee et al. [10] measured for their $Cu/ZnO/Al_2O_3$ catalysts. The combined adsorption constant $K^*_{HCOO^{(A)}}$ is two orders of magnitude higher than the value published by Peppley et al. This discrepancy may be explained by the fact that this group did not observe carbon dioxide inhibition of SRM over their commercial catalyst. Lee et al. also did not observe this kind of inhibition and included neither a formate nor a carbon dioxide adsorption term in their kinetic model, indicating that even among $Cu/ZnO/Al_2O_3$ systems, the relationship between different surface species can differ strongly. However, because in our DRIFTS study we did not observe a molecularly adsorbed CO_2 species but did find an inhibiting influence of this product gas on the SRM reaction, we assume carbon dioxide adsorption via carbonate formation, in agreement with a recent study [27].

As mentioned above, the $Cu/Cr_2O_3/Fe_2O_3$ catalyst CCF exhibited different behavior in SRM than the other three catalysts tested. The dependence of the rate on the feed composition indicated an RDS beyond methoxy dehydrogenation and including the participation of water or hydroxyl groups. This is shown in Fig. 9 for SRM over CZA and CCF applying a varying binary feed composition of water and methanol without the addition of inert or product gases.

The important difference between the curve shape for CCF and that of the other three catalysts is the plateau of the SRM reaction rate from 40 up to 80% methanol in the binary feed and the subsequent significant decrease. Because of to this shape, the reaction could not be fitted sufficiently with the mechanistic rate law in Eq. (7). Against this, the rate of SRM over CZA steadily increased with increasing methanol partial pressure up to 90% methanol in the feed, which exactly fits the general shape of this function.

The DRIFTS experiments showed that especially CCF was covered with a relatively high amount of formate groups. These results lead to the conclusion that formate dehydration was noticeably slower on this catalyst than on the other catalysts, maybe singularly rate-determining but definitely involved in the total rate. The mechanistic rate equation assuming formate de-

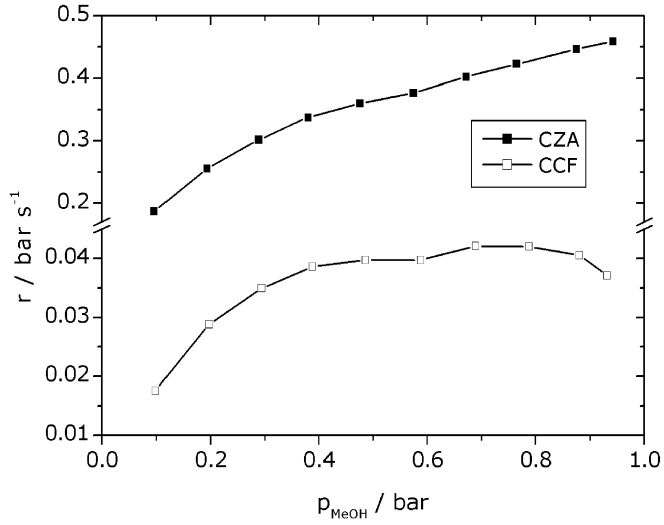

Fig. 9. Comparison of the dependence of SRM reaction rate over CZA and CCF on the feed composition without addition of inert or product gases, $T = 220\,^{\circ}\mathrm{C}$.

hydration (FDH) as the RDS in the catalysis cycle described in Fig. 7 is given by

$$r_{\mathrm{FDH}} = \Big(k_{\mathrm{FDH}} C^{\mathrm{T}}_{\mathrm{S_A}} \big(C^{\mathrm{T}}_{\mathrm{S_B}}\big)^6 \prod_i K_i^* \big(p_{\mathrm{CH_3OH}} p_{\mathrm{H_2O}} / p_{\mathrm{H_2}}^{5/2}\big)\Big) \Big/ \Big(\Big(1 + \underbrace{K^*_{\mathrm{CH_3O^{(A)}}} \big(p_{\mathrm{CH_3OH}} / p_{\mathrm{H_2}}^{1/2}\big)}_{\text{methoxy}} + \underbrace{K^*_{\mathrm{OH^{(A)}}} \big(p_{\mathrm{H_2O}} / p_{\mathrm{H_2}}^{1/2}\big)}_{\text{hydroxy}} + \underbrace{\prod_i K_i^* \big(p_{\mathrm{CH_3OH}} p_{\mathrm{H_2O}} / p_{\mathrm{H_2}}^{5/2}\big)}_{\text{formate}} + \underbrace{K_{\mathrm{CO_2^{(A)}}} p_{\mathrm{CO_2}}}_{\text{carbon dioxide}}\Big) \times \big(1 + K^{1/2}_{\mathrm{H^{(B)}}} p_{\mathrm{H_2}}^{1/2}\big)^6\Big), \tag{14}$$

where $\prod_i K_i^*$ represents the product of the equilibrium constants of all elemental reaction steps in the catalysis cycle from methanol adsorption up to dioxomethylene dehydrogenation. (The rate law following the methyl formate route is the same with respect to its algebraic form but with different meaning of its parameters.) Obviously, this product of six factors prevents meaningful fitting of experimental data, and thus the following discussion is only qualitative. As can be seen, this rate law describes in the differential conversion regime ($p_{\mathrm{H_2}}$, $p_{\mathrm{CO_2}} \approx 0$) a zero-order reaction over a wide range of feed compositions. However, against the rate law with methoxy dehydrogenation as the RDS, this rate law predicts a decreasing rate with the decrease of water in the feed, which is exactly the observed result.

Applying Eq. (14) for fitting the rate data acquired from CCF could be better fitted than with Eq. (7), but still not in a sufficiently high quality. Because the experimental data, displayed in Fig. 7, seems to result from a combination of both fundamental rate equation shapes, a combined rate equation is proposed for the final description,

$$\frac{1}{r} = \frac{1}{r_{\mathrm{MDH}}} + \frac{1}{r_{\mathrm{FDH}}}, \tag{15}$$

which is the expression corresponding to Kirchhoff's law of electricity, implying that the total rate is affected mainly by the slowest of both elemental reactions, methoxy and formate dehydrogenation, the activation barriers of which may be comparable to electronic resistors. Unfortunately, only the general shape of the results can be explained using this model. The high reaction order of hydrogen in r_{FDH} predicts an immense inhibition of the reaction progress by its appearance, which actually is not observed to this extent in the experimental results. This produces unrealistically low values for the hydrogen adsorption constant $K_{\mathrm{H^{(B)}}}$ and thereby high values for the product $\prod_i K_i^*$, although the rate data fit is sufficiently accurate. The values of the fitted parameters are not presented here. However, the assumption that SRM over CCF has a second barrier at formate dehydrogenation is also confirmed by its low selectivity. Compared with the other three catalysts, CCF produced a high amount of CO in the product stream, which must have formed from an intermediate preliminary to formate, because formate itself decomposes directly into the main reaction products H_2 and CO_2. Millar et al. [42] and Fisher and Bell [44] reported CO formation from methyl formate in the absence of water. Although not observed in the DRIFTS studies, increased CO production may indicate a higher amount of methyl formate on the surface due to slower formate dehydrogenation.

Due to the differences in catalytic behavior, it was considered necessary to prove that the SRM catalysis over CCF involves copper as an active phase, because Fe_2O_3/Cr_2O_3 systems are known to be active for water–gas shift catalysis and a certain activity in SRM may be considered possible. To determine the activity as a function of copper content, catalyst samples with different compositions were synthesized. The ratio of Cr_2O_3 and Fe_2O_3 was kept constant at the value given by CCF, whereas the copper content was varied from 0 to 6%. The activity in SRM was determined at 300 °C and an equimolar methanol/water feed of 0.5 ml min^{-1}. The conversions thus observed were related to the BET surface areas of the samples. A linear correlation of this modified activity and the copper content of the sample was expected from Eq. (8) and was observed, as shown in Fig. 10.

This result is a clear indication that copper or a copper-containing phase formed in these samples was responsible for the catalytic activity. Because the copper-free sample provided nearly no activity, the contribution of the Fe_2O_3/Cr_2O_3 catalyst support to the measured conversion can be neglected. The linear increase in this low-concentration range indicates the formation of uniform and uniformly sized copper particles.

In an early stage of this study, it was observed that the $Cu/Cr_2O_3/Fe_2O_3$ high-temperature-shift catalyst exhibited remarkably low activity and poor selectivity for SRM, and this combination will definitely never reach technical application for this reaction. However, this catalyst was not suspended from further experiments, because there is a pool of information about a reaction system that cannot be discovered by the analysis and investigation of good and optimized catalysts. The knowledge of reasons why particular systems (e.g., CCF as a catalyst for SRM) do not operate in the expected way sometimes provides

deeper insight into and better understanding of the systems that work well.

Vargas et al. [27] recently proposed that methanol adsorption during SRM occurs on oxidized surface sites independent of the presence of oxygen in the feed. They posited that these sites in the absence of oxygen are formed via dissociative water adsorption, especially at low temperatures (<250 °C). A kinetic evaluation of this pathway inevitably should result in a much stronger influence of water concentration on the SRM reaction rate than was actually found in our study. From a kinetic standpoint, this mechanism could not be adapted to our experimental results. However, their DRIFT study was conducted at even higher temperatures, up to 450 °C. Despite these contradictions, Vargas et al. also identified the selectivity-determining step between methoxy and formate intermediates, which is in agreement with our results. Enhanced CO formation via formate decomposition [27], as well as methyl formate decomposition [42,44], match well with the higher amount of formate groups on CCF and the resulting poor selectivity toward CO_2. Indeed, a recent kinetic study on the SRM reaction network over CCF (B. Frank, unpublished results) indicated that CO formation over this catalyst occurred mainly via methanol decomposition, whereas the main source of CO over CZA and CZC was the rWGS reaction [5,8].

3.4.3. Power law fit

Because of their easier handling, power rate laws are often used for sizing reactors in industrial and technical sciences [45–47]. An interesting difference among several power rate laws given in the literature is found in the inhibiting effect of carbon dioxide. Jiang et al. [31] and Lee et al. [10] could not measure any inhibition of carbon dioxide on SRM over $Cu/ZnO/Al_2O_3$ catalysts. In contrast, Idem and Bakhshi [48] and Samms and Savinell [49] found such an inhibition over their copper catalysts. For technical applications, this differentiation between two inhibiting species is of no importance, because hydrogen and carbon dioxide are formed at a strict stoichiometric ratio of 3, and their exponents can be transformed algebraically. But from a mechanistic standpoint, this finding may be very important, as was shown earlier.

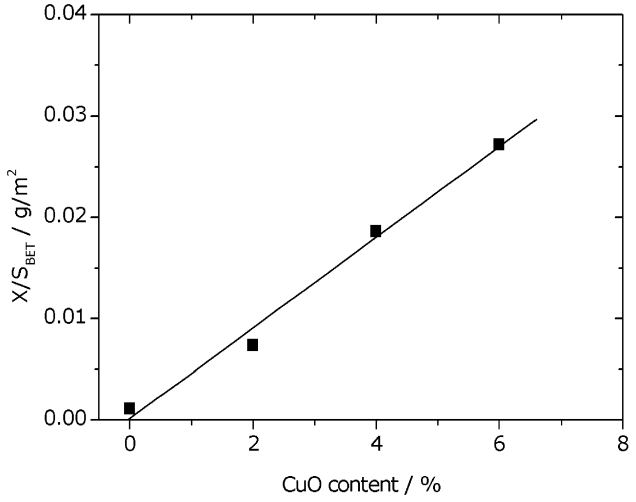

Fig. 10. Dependence of the surface area related SRM activity of $CuO/Cr_2O_3/Fe_2O_3$ catalyst samples from their copper oxide content.

Because many kinetic studies reported in the literature are based on simple power rate laws, we completed our investigation with a power law fit of the kinetic data, to allow a better comparison with the results of research groups who published only power law fits. The reaction orders of methanol (n_M), water (n_W), hydrogen (n_H), and carbon dioxide (n_C) were fitted to the complete dataset of about 200 data points for each catalyst with a rate expression of the following form:

$$r = k p_{CH_3OH}^{n_M} p_{H_2O}^{n_W} p_{H_2}^{n_H} p_{CO_2}^{n_C}, \tag{16}$$

where r is the reaction rate of methanol consumption (bar s^{-1}), k is the rate constant (bar^x s^{-1} with $x = 1 - \sum n_i$), p_i is the partial pressure (bar), and n_i is the reaction orders of the reactants.

As expected from the mechanistic modeling, we found that the reaction rate was determined mainly by the methanol partial pressure, whereas the reaction order of water was very low for all catalysts. Both main reaction products were found to inhibit the reaction, which is expressed in negative reaction orders. The reaction order of nitrogen n_N was found to be 0 ± 0.02, as expected, and the range of ± 0.02 may indicate the experimental error of our investigation. The results of the power law fit are given in Table 6.

Lee et al. [10] used a power expression for hydrogen of the type $(A + p_{H_2})^{n_H}$ to undergo infinite reaction rates at the reactor inlet, where the partial pressure of hydrogen is zero. For numerical fitting, we solved this mathematical problem by initializing the hydrogen partial pressure with an extremely small value of 10^{-5} bar. Indeed, the variation of this initialization parameter in the range of 10^{-4}–10^{-7} bar causes a negligible deviation of the predicted methanol conversion of <0.1%.

As shown in Table 6, the reaction order of water is the highest on CCF. This is in good agreement with the results of the mechanistic study, because on this catalyst, the effect of the water partial pressure is relatively high, due to the influence of formate dehydrogenation on the overall reaction rate. The water reaction orders are slightly positive on CZA, CZC, and CS

Table 6
Rate constants and reaction orders of SRM over the investigated copper-containing catalysts measured at 220 °C

Catalyst	k [bar^x s^{-1}]	n_M	n_W	n_H	n_C	n_N	R^2
CZA	0.117 ± 0.004	0.491 ± 0.012	0.021 ± 0.008	-0.31 ± 0.01	-0.082 ± 0.005	-0.021 ± 0.008	0.963
CCF	0.034	0.52	0.11	−0.19	−0.09	−0.01	
CZC	0.062 ± 0.002	0.603 ± 0.010	0.032 ± 0.006	-0.319 ± 0.007	-0.173 ± 0.005	0.017 ± 0.005	0.979
CS	0.0245 ± 0.007	0.567 ± 0.009	0.048 ± 0.005	-0.266 ± 0.006	-0.110 ± 0.004	-0.01 ± 0.01	0.980

against the slightly negative reaction order, as predicted by the pure application of Eq. (7). This also may indicate a slight influence of formate dehydrogenation on the SRM reaction rate on these catalysts.

3.5. Apparent activation energy and comparison of activity

From the temperature dependence of the reaction rate, the apparent activation energy was calculated from the slope of the dataset in an Arrhenius plot (Fig. 11). Linearity was observed for each catalyst, indicating no change in the RDS or diffusion limitation over the temperature range investigated. This figure also gives a clear comparison of the activities of the catalysts. The activation energies, E_A, determined from the Arrhenius plot and the reaction rate at 220 °C are given in Table 7.

The activation energies of SRM over CZC and CS were nearly identical, in agreement with our assumption of the same RDS. The temperature dependence over CZA was slightly lower, but this can be attributed to the high copper content of this sample, as shown in a previous study [5]. A clear difference in the activation energy was observed for CCF; this value was noticeably low, indicating a difference in the RDS as described in detail above. An extremely low value of E_A for SRM over a $Cu/Cr_2O_3/Fe_2O_3$ water–gas shift catalyst was also found by Löffler et al. [50].

Because there are no comparable data on the influence of the catalyst support on the activity in SRM, we compared the activities referred to the mass of copper with specific activities found for methanol synthesis given by Fujitani et al. [51]. Those authors found that the specific activity of copper-based catalysts depends on the support in the decreasing order $Cr_2O_3 > ZrO_2 \approx Al_2O_3 > SiO_2$ and observed a promoting effect of ZnO on each support. Taking into account that our $Cu/ZnO/Al_2O_3$ catalyst was up to 5 times less active than other systems reported (see Section 3.1), these results are in good agreement. Although there are, of course, significant differences in the copper loading of our catalysts, and the influence of Fe_2O_3 and CeO_2 was neglected in this comparison, this may indicate the similarity of the active sites of copper-based catalysts used in methanol synthesis and SRM.

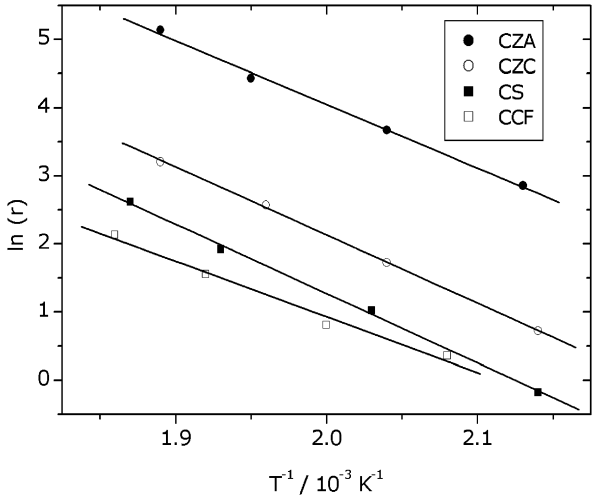

Fig. 11. Arrhenius plot for SRM over the investigated copper catalysts in the temperature range of 200–250 °C ($m_{CZA} = 0.5$ g, $m_{CCF} = 2.5$ g, $m_{CZC} = 1.0$ g, $m_{CS} = 2.0$ g, $p = 1$ bar, $w = 0.3$–2 ml min^{-1}, $MeOH/H_2O = 1$, reaction rate r in mmol s^{-1} kg^{-1}).

Table 7
Activation energies and reaction rates at 220 °C of copper-based catalysts expressed for overall catalyst amount and Cu-content

Sample	E_A [kJ mol^{-1}]	r_{220} [mmol kg$_{cat}^{-1}$ s^{-1}]	r_{220} [mmol kg$_{Cu}^{-1}$ s^{-1}]
CZA	76.9	44.1	80.3
CCF	67.4	2.0	100.2
CZC	84.9	6.4	92.2
CS	85.7	2.6	22.5

4. Conclusion

The reaction mechanism of SRM was investigated in detail by means of a kinetic study based on the differential method. The proposed reaction mechanism, based on previous studies, was supported by a DRIFTS study. Microkinetic measurements were conducted, taking the elimination of mass transfer limitation, as well as experimental errors and result falsification due to catalyst aging, into account.

The elementary reaction steps occurring on the surfaces of copper catalysts during SRM were found to be similar and independent of the catalyst support. As reported by several authors, the dehydrogenation of methoxy groups was found to be the RDS of this reaction over $Cu/ZnO/Al_2O_3$ catalysts. This insight was extended to Cu/SiO_2 and $Cu/ZrO_2/CeO_2$ systems, which showed identical reaction rate dependence on the feed composition. Kinetic constants were found to be in the same order of magnitude for each catalyst. The surfaces of all catalysts were dominated by methoxy and formate groups; the intermediates formaldehyde, dioxomethylene, and methyl formate were not observed. Because methyl formate appeared in the product spectrum only at high methanol surplus, a change in the reaction pathway from the dioxomethylene to the methyl formate route is assumed, depending on the water content in the feed. A strong signal of formate groups in the DRIFT spectrum indicates relatively slow decomposition of these species into the reaction products. This does not affect the reaction rate over the $Cu/ZnO/Al_2O_3$, Cu/SiO_2, and $Cu/ZrO_2/CeO_2$ catalysts investigated. Regarding the $Cu/Cr_2O_3/Fe_2O_3$ catalyst, this step was indeed found to decrease the overall reaction rate, and a combined rate was proposed considering methoxy and formate dehydrogenation as the two slowest elementary reaction steps. This significant finding was confirmed by a thorough evaluation of the corresponding band areas in the DRIFT spectra, as well as by the greater formation of the byproduct CO over this catalyst, which is probably formed by the decomposition of methyl formate, the surface intermediate preliminary to formate in the supposed catalysis cycle. A particularly low apparent SRM activation energy over CCF compared with CZA, CZC, and CS also confirms the assumption of a change in the RDS on this catalyst.

Acknowledgments

Financial support by the ZEIT Foundation (Project "Nanochemistry for the Automobiles of the Future" (http://www.zeit-stiftung.de)) is gratefully acknowledged. The authors thank Dr. Ágnes Mastalir, University of Szeged, for helpful discussions.

References

[1] A. Chambers, C. Park, R.T.K. Baker, N.M. Rodriguez, J. Phys. Chem. B 102 (1998) 4253.
[2] B. Lindström, L.J. Petterson, Int. J. Hydrogen Energy 26 (2001) 923.
[3] G. Jacobs, B.H. Davis, Appl. Catal. A 285 (2005) 43.
[4] G.A. Olah, Catal. Lett. 93 (2004) 1.
[5] A. Mastalir, B. Frank, A. Szizybalski, H. Soerijanto, A. Deshpande, M. Niederberger, R. Schomäcker, R. Schlögl, T. Ressler, J. Catal. 230 (2005) 464.
[6] B.A. Peppley, J.C. Amphlett, L.M. Kearns, R.F. Mann, Appl. Catal. A 179 (1999) 21.
[7] B. Lindström, L. Petterson, J. Power Sources 118 (2003) 71.
[8] H. Purnama, T. Ressler, R.E. Jentoft, H. Soerijanto, R. Schlögl, R. Schomäcker, Appl. Catal. A 259 (2004) 83.
[9] B.A. Peppley, J.C. Amphlett, L.M. Kearns, R.F. Mann, Appl. Catal. A 179 (1999) 31.
[10] J.K. Lee, J.B. Ko, D.H. Kim, Appl. Catal. A 278 (2004) 25.
[11] S.A. Asprey, B.W. Wojciechowski, B.A. Peppley, Appl. Catal. A 179 (1999) 51.
[12] M.P. Harold, B. Nair, G. Kolios, Chem. Eng. J. 58 (2003) 2551.
[13] A. Morillo, A. Freund, C. Merten, Ind. Eng. Chem. Res. 43 (2004) 4624.
[14] F. Gallucci, L. Paturzo, A. Basile, Ind. Eng. Chem. Res. 43 (2004) 2420.
[15] C.J. Jiang, D.L. Trimm, M.S. Wainwright, N.W. Cant, Appl. Catal. A 97 (1993) 145.
[16] K. Takahashi, N. Takezawa, H. Kobayashi, Appl. Catal. 2 (1982) 363.
[17] Y. Choi, H.G. Stenger, Appl. Catal. B 38 (2002) 259.
[18] Y. Liu, T. Hayakawa, K. Suzuki, S. Hamakawa, T. Tsunoda, T. Ishii, M. Kumagai, Appl. Catal. A 223 (2002) 137.
[19] N. Takezawa, N. Iwasa, Catal. Today 36 (1997) 45.
[20] K. Takahashi, N. Takezawa, H. Kobayashi, Chem. Lett. (1985) 759 (cited in [19]).
[21] J. Skrzypek, J. Sloczynki, S. Ledakowicz, Methanol Synthesis, ISBN 83-01-11490-8, Polish Scientific Publishers, Warsaw, 1994 (cited in [9]).
[22] R.J. Burch, S.E. Golunski, M.S. Spencer, Catal. Lett. 5 (1990) 55.
[23] K.D. Jung, A.T. Bell, J. Catal. 193 (2000) 207.
[24] J. Agrell, H. Birgersson, M. Boutonnet, I. Melián-Cabrera, R.M. Navarro, J.L.G. Fierro, J. Catal. 219 (2003) 389.
[25] J.P. Breen, F.C. Meunier, J.R.H. Ross, Chem. Commun. (1999) 2247.
[26] P.H. Matter, U.S. Ozkan, J. Catal. 234 (2005) 463.
[27] M.A.L. Vargas, G. Busca, U. Costantino, F. Marmottini, T. Montanari, P. Patrono, F. Pinzari, G. Ramis, J. Mol. Catal. A (2006), doi:10.1016/j.molcata.2006.08.085.
[28] A.S. Deshpande, N. Pinna, P. Beato, M. Antonietti, M. Niederberger, Chem. Mater. 16 (2004) 2599.
[29] L. Trouillet, T. Toupance, F. Villain, C. Louis, Phys. Chem. Chem. Phys. 2 (2000) 2005.
[30] J.M. Coulson, J.F. Richardson, R.K. Sinnott, Chemical Engineering, vol. 6, Pergamon, Oxford, 1983, p. 253.
[31] C.J. Jiang, D.L. Trimm, M.S. Wainwright, N.W. Cant, Appl. Catal. A 93 (1993) 245.
[32] M. Baerns, H. Hofmann, A. Renken, Chemische Reaktionstechnik, third ed., Thieme, Stuttgart, 1999 (in German).
[33] J.R. Katzer, dissertation, Massachusetts Institute of Technology, Cambridge, Massachusetts, 1969 (cited in [32]).
[34] M. Kurtz, H. Wilmer, T. Genger, O. Hinrichsen, M. Muhler, Catal. Lett. 86 (2003) 77.
[35] M.V. Twigg, M.S. Spencer, Top. Catal. 22 (2003) 191.
[36] X. Zhang, P. Shi, J. Mol. Catal. A 194 (2003) 99.
[37] A. Szizybalski, F. Girgsdies, A. Rabis, Y. Wang, M. Niederberger, T. Ressler, J. Catal. 233 (2005) 297.
[38] V. Agarwal, S. Patel, K.K. Pant, Appl. Catal. A 279 (2005) 155.
[39] D.B. Clarke, D.K. Lee, M.J. Sandoval, A.T. Bell, J. Catal. 150 (1994) 81.
[40] D.M. Monti, N.W. Cant, D.L. Trimm, M.S. Wainwright, J. Catal. 100 (1986) 17.
[41] R. Zhang, Y. Sun, S. Peng, Fuel 11–12 (2002) 1619.
[42] G.J. Millar, C.H. Rochester, K.C. Waugh, J. Chem. Soc. Faraday Trans. 87 (1991) 2795.
[43] G. Busca, A.S. Elmi, P. Fortazzi, J. Phys. Chem. 91 (1987) 5263.
[44] I.A. Fisher, A.T. Bell, J. Catal. 184 (1999) 357.
[45] J. Agrell, H. Birgersson, M. Boutonnet, J. Power Sources 4654 (2002) 1.
[46] P. Reuse, A. Renken, K. Haas-Santo, O. Görke, K. Schubert, Chem. Eng. J. 102 (2004) 133.
[47] L. Ma, C. Jiang, A.A. Adesina, D.L. Trimm, M.S. Wainwright, Chem. Eng. J. 62 (1996) 103.
[48] R.O. Idem, N.N. Bakhshi, Chem. Eng. Sci. 51 (1996) 3697.
[49] S.R. Samms, R.F. Savinell, J. Power Sources 112 (2002) 13.
[50] D.G. Löffler, S.D. McDermott, C.N. Renn, J. Power Sources 114 (2003) 15.
[51] T. Fujitani, M. Saito, Y. Kanai, T. Kakumoto, T. Watanabe, J. Nakamura, T. Uchijima, Catal. Lett. 25 (1994) 271.
[52] C.T. Wang, R.J. Willey, J. Catal. 202 (2001) 211.